Electronic Supplementary Material (ESI) for Chemical Science.
This journal is © The Royal Society of Chemistry 2021

A core-brush 3D DNA nanostructure: the next generation of DNA nanomachine for ultrasensitive sensing and imaging of intracellular microRNA with rapid kinetics

Lingqi Kong, Beibei Kou, Xiaolong Zhang, Ding Wang, Yali Yuan, Ying Zhuo, Yaqin Chai*, and Ruo Yuan**

Key Laboratory of Luminescence and Real-Time Analytical Chemistry (Southwest University), Ministry of Education, College of Chemistry and Chemical Engineering, Southwest University, Chongqing 400715, People's Republic of China.

* Corresponding author. Tel.: +86-23-68252277; Fax: +86-23-68253172

E-mail address: yqchai@swu.edu.cn (Y. Q. Chai); yuanruo@swu.edu.cn (R. Yuan)

Table of Contents

Materials and reagents.

Tris (2-carboxyethy) phosphine hydrochloride (TCEP), 6-mercapto-1-hexanol (MCH) and Gold chloride ($HAuCl_4 \cdot 4H_2O$) were purchased from Sigma-Aldrich (St. Louis, MO, U.S.A). N-(3-Dimethylaminopropyl)-N′-ethylcarbodiimide hydrochloride (EDC) and N-Hydroxy succinimide (NHS) were acquired from Shanghai Medpep Co. (Shanghai, China). T4 DNA ligase and Phi29 DNA polymerase were obtained from Vazyme Biotech Company, Ltd. (Nanjing, China). Deoxynucleotides (dNTPs) was bought from Genview Scientific Inc. (El Monte, CA, U.S.A.). Magnetic nanobeads (MNB) were provided by Tianjin Unibead Scientific Company, Ltd. (Tianjin, China). $MgCl_2 \cdot 6H_2O$, $Pb(NO_3)_2$, $CuCl_2$, $CaCl_2$, $MnCl_2$, and $Zn(NO_3)_2 \cdot 6H_2O$ were obtained from Chengdu Kelong Company Ltd. (Chengdu, China). 5 × TBE buffer (0.25 M H_3BO_3, 0.01 mM EDTA, 0.25 M Tris, pH 8.0) was employed to the polyacrylamide gel electrophoresis (PAGE) experiments. Gel red nucleic acid dye was acquired from Sangon Biotech Co., Ltd. (Shanghai, China) for gel imaging. Dulbecco's Modified Eagle Medium (DMEM) and 4% paraformaldehyde were bought from Thermo Fisher Scientific Inc. (Shanghai, China) for cell experiment. Phosphate buffered solution (PBS, pH 7.0, 0.1 M) were prepared by mixing the solutions of 0.1 M Na_2HPO_4, 0.1 M KH_2PO_4 and 0.1 M KCl. Ultrapure water was applied during the entire experiments (18.2 MΩ/cm at 25 °C). 20 mM Tris-HCl buffer (pH 7.4) containing 140 mM NaCl, 1 mM $CaCl_2$ and 5 mM KCl was used to prepare DNA oligonucleotide solution. The oligonucleotides were custom-synthesized by Sangon Biotech Co., Ltd. (Shanghai, China) with the sequences listed in Table S1.

Table S1. Oligonucleotide sequences.

Names	Sequences (5'-3')
primer	CAG ATG GTA GCG GTT CAG ATG GTA G
padlock	PO_4-CCG CTA CCA TCTG AA CGT CCG TCA GTAC AA CCG CTA CCA TCTG AA CCG CTA CCA TCTG AA
L	GAA GAG ATC AAC ATC AGT C TG ATA AGC TA
HS	CCG CTA CCA TCT GT/BHQ/ GCT GTG TAA CTA T/rA/G GAA GAG ATC ACA GC-NH_2
HS-1	CCG CTA CCA TCT GT/BHQ/ GCT GTG TAA CTA T/rA/G GAA GAG ATC ACA GC-FAM
HS-2	SH-CCG CTA CCA TCT GTG CTG TGT AAC TAT /rA/GG AAG AGA TCA CAG C-FAM
DA-25T	CGT CCG TCA GTA CTT TTT TTT TTT TTT TTT TTT TTT TTG ACT GAT GTT GAT CTC TTC TCC GAG CCG GTC GAA ATA GTT
DA-30T	CGT CCG TCA GTA CTT TTT TTT TTT TTT TTT TTT TTT TTT TTT TGA CTG ATG TTG ATC TCT TCT CCG AGC CGG TCG AAA TAG TT
DA-35T1	CGT CCG TCA GTA CTT TTT TTT TTT TTT TTT TTT TTT TTT TTT TTT GAC TGA TGT TGA TCT CTT CTC CGA GCC GGT CGA AAT AGT T
DA-35T2	SH-CGT CCG TCA GTA CTT TTT TTT TTT TTT TTT TTT TTT TTT TTT TTT GAC TGA TGT TGA TCT CTT CTC CGA GCC GGT CGA AAT AGT T
DA-40T	CGT CCG TCA GTA CTT TTT TTT TTT TTT TTT TTT TTT TTT TTT TTT TTT TTG ACT GAT GTT GAT CTC TTC TCC GAG CCG GTC GAA ATA GTT
DA-45T	CGT CCG TCA GTA CTT TTT TTT TTT TTT TTT TTT TTT TTT TTT TTT TTT TTT TTT TGA CTG ATG TTG ATC TCT TCT CCG AGC CGG TCG AAA TAG TT
DA-50T	CGT CCG TCA GTA CTT TTT TTT TTT TTT TTT TTT TTT TTT TTT TTT TTT TTT TTT TTT GAC TGA TGT TGA TCT CTT CTC CGA GCC GGT CGA AAT AGT T
H	SH-GCT GTG ATC TCT TCC TTA ACT TAA GAG ATC
miRNA-21	UAG CUU AUC AGA CUG AUG UUG A
miRNA-155	UUA AUG CUA AUC GUG AUA GGG GU
miRNA-126	CAU UAU UAC UUU UGG UAC
miRNA-141	UAA CAC UGU CUG GUA AAG AUG G

miRNA-203a	AGU GGU UCU UAA CAG UUC AAC AGU U
miRNA-182-5P	UUU GGC AAU GGU AGA ACU CAC ACU

Apparatus and measurements.

The ECL measurements was recorded on a MPI-A multifunctional analyzer (Xi'An Remax Electronic Science & Technology Co. Ltd., Xi'An, China). Cyclic Voltammetry (CV), Electrochemical Impedance Spectroscopy (EIS), and chronocoulometry (CC) were accomplished by a CHI760E electrochemical workstation (CH Instruments, Shanghai, China) with a three-electrode arrangement. Native polyacrylamide gel electrophoresis (PAGE) was carried out with BG-verMIDI standard vertical electrophoresis apparatus (Baygene, Beijing, China) and the gel imaging was accomplished by a Bio-Rad imaging System (Bio-Rad, Hercules, CA, U.S.A.). The fluorescent responses were obtained by a FL-7000 fluorescence spectrophotometer (Hitachi, Tokyo, Japan) with the PMT voltage and the slit width set as 950 V and 5.0 nm respectively. Fluorescence imaging of living cells was used by an Olympus IX-81 microscope equipped with a Total Internal Reflection Fluorescence (TIRF) microscopy (Olympus, Japan). Ultraviolet-visible (UV-*vis*) absorption spectrums were accomplished with UV-2450 UV-vis spectrophotometer (Shimadzu, Tokyo, Japan) and atomic force microscope (AFM) was carried on a multimode 8 microscope (Bruker, Germany).

Construction of the core-brush 3D DNA nanomachine.

At first, 5 μL of EDC and NHS (4:1) was added into 25 μL of cleaned carboxyl-

MNB suspension and stirred for 45 min to activate the carboxyl. Next, 25 μL 2 μM the aminated DNA primer was mixed with the activated MNB suspension at room temperature for 4 h to obtain DNA primer-functionalized MNB suspension. The resulting suspension was subjected to magnetic separation, washed twice with PBS buffer and then dispersed in 25 μL PBS buffer. Following that, the padlock (25 μL 0.6 μM) was added into the primer-MNB suspension, and then subsequently annealed at 95 °C for 10 min. The resulting suspension was magnetic separated and dispersed in the mixture of 3 μL 10 × T4 DNA ligase buffer, 1 μL T4 DNA ligase (400 U/μL) and 21 μL Tris-HCl buffer. Then the solution was incubate at 16 °C for 6 h and thermally treated at 65 °C for 12 min to inactivate the T4 DNA ligase. Afterwards, the mixture was incubated with Phi29 DNA polymerase (1 U/μL), 1 × Phi29 reaction buffer and dNTPs (2 mM) for 2 h at 37 °C and then handled at 65°C for 10 min to denature the Phi29 DNA polymerase. With the accomplishment of RCA reaction, the long DNA track was generated on MNB. In order to ensure the DNAzyme walking arm (DA) was locked completely, the locking strand (L) and DA were mixed at a molar ratio of 3:1 to generate the DA-L complex. Moreover, $Ru(bpy)_2^{2+}$ was introduced to a mixture of EDC and NHS (4:1) for 45 min to activate the carboxyl. hairpin substrate (HS) modified with amino was added to the above solution and stirred for 4 h to obtain the conjugate of HS- $Ru(bpy)_2^{2+}$. Subsequently, the locked DA and HS- $Ru(bpy)_2^{2+}$ (molar ratio of 3:1) were conjugated to the DNA track-MNB at 37 °C for 2 h to obtain the prepared core-brush 3D DNA nanomachine, in which the MNB was core and the DNA track assembled with DNA components was brush.

Cell Culture and Cell Lysate Preparation.

The MCF-7 cells (human breast cancer cells) and HeLa cells (human cervical cancer cells) were purchased from the cell bank of the Chinese Academy of Sciences (Shanghai, China). The MCF-7 and HeLa cells were cultured in DMEM medium containing 100 U/mL penicillin, 10% fetal bovine serum (FBS) and 1% non-essential amino acids at 37 °C with a humidified atmosphere (95% air and 5% CO_2). Then, the total RNA extraction for the real sample detection was obtained using the Trizol Reagent Kit (Invitrogen Biotechnology Co., Ltd) according to the manufacturer's protocol. Firstly, the cell pellets were added to appropriate Trizol Reagent and oscillate three times. Then, the processed cell pellets were transferred to an RNase-free centrifuge tube and incubated at room temperature for 5-10 min to ensure complete cell disruption. Afterwards, the processed RNA pellets were washed with 75% ethanol and re-dissolved in RNase-free water after, and stored at -20 °C for further use.

Polyacrylamide-gel electrophoresis (PAGE).

Firstly, the DNA samples were mixed with the 6 × loading buffer at a volume ratio of 5:1, then the mixtures were analyzed by polyacrylamide-gel electrophoresis (PAGE) on a freshly prepared 8% polyacrylamide gel in 1 × TBE buffer at 60 mA for 1 h. After being stained by Gel Red for 10 min, the gel was performed in the Bio-Rad imaging system (Hercules, CA, USA) to get the electrophoresis results.

TIRF microscopy imaging of miRNAs in living cells.

The procedures for miRNA imaging using TIRF microscopy were as follows. At

first, the MCF-7 and HeLa cells were introduced into a 35 mm^2 Petri dish. Immediately, they were respectively cultured in DMEM medium with a humidified atmosphere (5% CO_2) at 37 °C for 24 h to reach 80% cell anchorage-dependent rate and then washed with sterile PBS. After that, the 50 μL 200 nM of the DNA nanomachine was separately incubated into MCF-7 cells Petri dish and HeLa cells Petri dish at 37 °C for 4 h to allow cell uptake of the DNA nanomachine. After washed with 25 mM Tris-acetate buffer (pH=8.0, 125 mM NaCl) for three times to remove excess nanomachine. These cells were subsequently treated with the 25 mM Tris-acetate buffer (pH 8.0, 125 mM NaCl and 15 mM $MnCl_2$) to allow the cellular uptake of Mn^{2+}. Then, the cells were stained with a Hoechst 33342 solution for 12 min and washed three times with 1 × PBS. After that, the cells were incubated with 1 mL of fresh DMEM medium at 25 °C before fluorescence imaging.

To modulate intracellular expression of miRNA-21, MCF cells were incubated with containing Lipofectanmine® 3000 and 300 nM synthetic miRNA-21 mimic or miRNA-21 inhibitor, respectively. These cells were imaged with TIRF according to the same procedures as above described. The transfection process was operated according to Lipofectanmine® 3000 DNA Transfection Reagent Protocol.

Particle size distribution and zeta potential analysis.

10 μL the MNB core or the core-brush 3D DNA nanomachine was added to 990 μL ultrapure water, respectively. The zeta potential measurements were conducted using a Brookhaven NanoBrook Omni zeta potential analyzer on the PALS mode at

room temperature. The measurements of hydrodynamic diameter were used a Brookhaven NanoBrook Omni instrument in the dynamic light scattering (DLS) mode at 25 °C. Each measurement was conducted 5 times for each of the prepared samples. Therefore, all zeta potential values and hydrodynamic diameter values are the average of 5 measurements.

AFM images of MNB core and core-brush 3D DNA nanomachine.

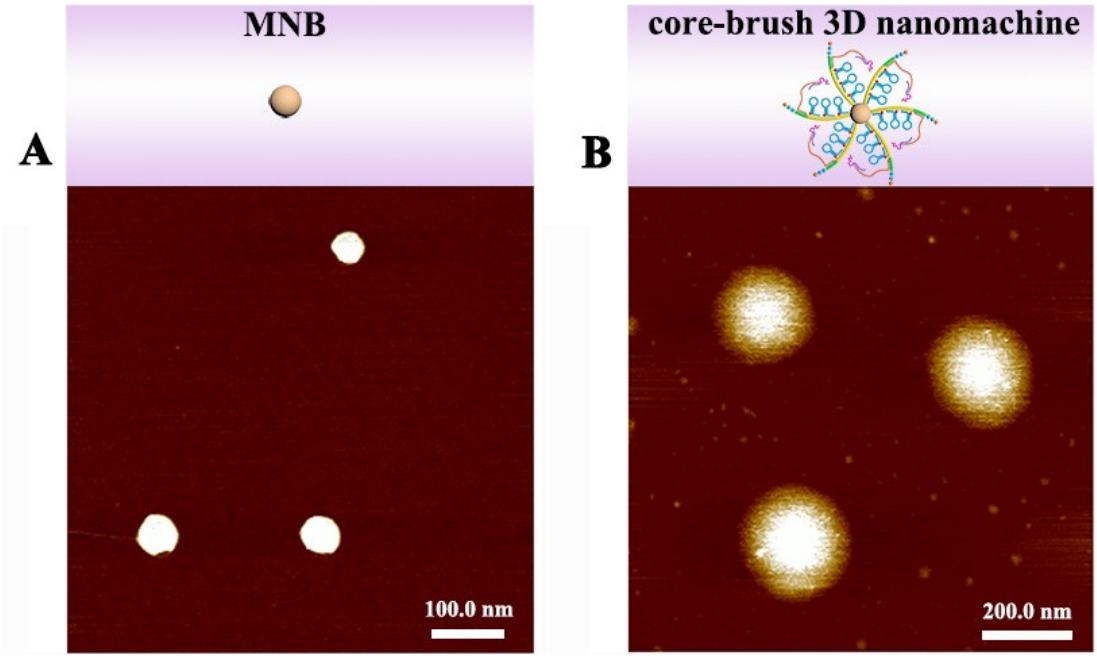

Fig. S1. AFM images of MNB core (A) and core-brush 3D DNA nanomachine (B), scale bars: 100 nm and 400 nm, respectively.

Investigation of the length of the DNAzyme arm.

The length of the DNAzyme arm (DA) was the critical factor affecting the walking efficiency of the proposed core-brush 3D DNA nanomachine. To better understand its influences, we first fixed the ratio of DA and HS-1 labelled with fluorophore (FAM)

and quenchers (BHQ) at 1:3, and then the fluorescence analysis was used to quantitatively investigate the dynamics performance of DA with different lengths (25T, 30T, 35T, 40T, 45T and 50T). As demonstrated in Fig. S2A, we monitored the fluorescence intensity of FAM of the proposed 3D DNA nanomachine assembled DA with different lengths in real-time within 2500 s. The saturation fluorescence intensity of FAM increased with the length of DA from 25T to 35T and decreased from 35T to 50T and reached the maximum at 35T, confirming that the DA-35T could provide sufficient spatial distance to perform nanomechanical movements for cleaving HS. Then, we further investigated the initial rate of the 3D DNA nanomachine assembled with different lengths of DA in Fig. S2B. Intuitively, the DA-35T had a relatively fast initial rate to achieve the optimal performance of the proposed 3D DNA nanomachine. Thus, the DA-35T was selected for subsequent experiments.

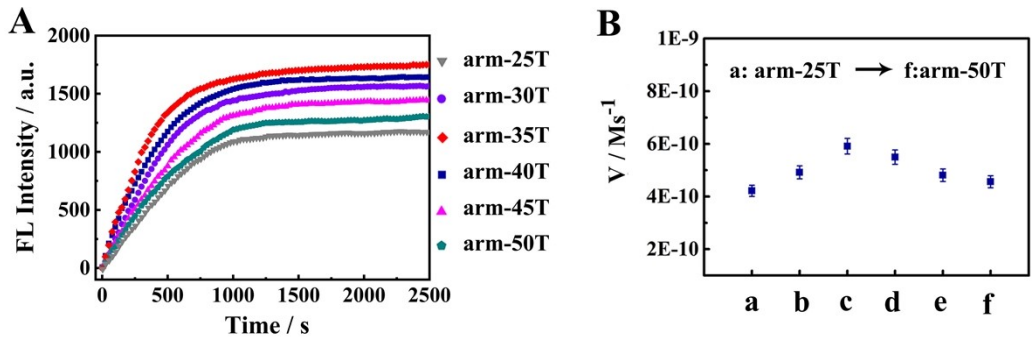

Fig. S2. (A) Real-time monitoring of fluorescence increase of the core-brush structured 3D DNA nanomachine with the length of the DA varying from 25T to 35T over a period of 2500 s. (B) The initial rate of the proposed 3D DNA nanomachine assembled with different length of the DA varying from 25T to 35T.

Optimization of the concentration of capture probe.

To obtain the optimal analytical performance of the developed sensing platform for miRNA-21 analysis, the concentration of capture probe H was optimized in Fig. S3. The ECL response continuously increase with the immobilization concentration of H from 1 μM to 3 μM, which was owing to the fact that more Ru-labelled segment (S) were captured by H onto the surface of modified electrode. Nevertheless, the ECL response decreased slightly with the immobilization concentration of H beyond 3 μM, which might be due to the increased steric hindrance of the high immobilization concentration of H. Thus, the optimized immobilization concentration of H was 3 μM.

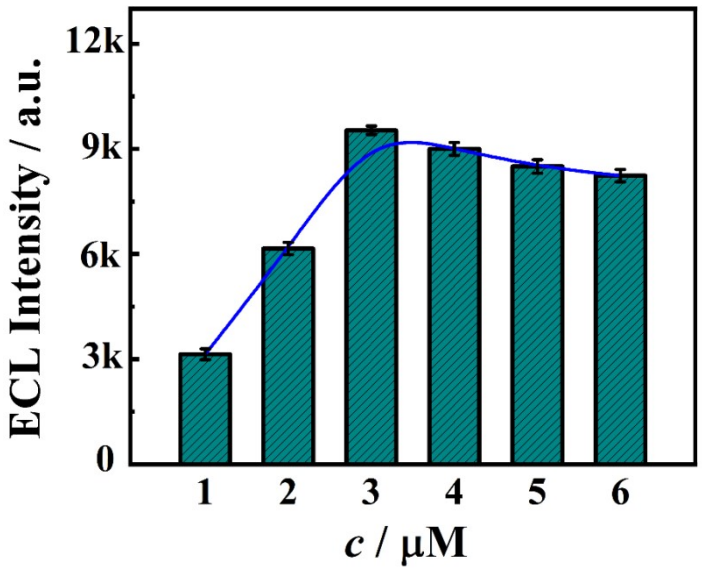

Fig. S3. The effect of the concentration of capture probe H on the proposed ECL biosensor.

Characterization of the electrode modification.

To investigate the stepwise fabrication process for the modified electrode, the cyclic voltammetry (CV) and electrochemical impedance spectroscopy (EIS) were performed in 5 mM $[Fe(CN)_6]^{3-/4-}$. As displayed in Fig. S4A, relative to the bare GCE (curve a), electrodeposition of the AuNPs generated an increasing redox peak current

(curve b) because AuNPs could facilitate electron transfer between the electrode and $[Fe(CN)_6]^{3-/4-}$. However, when the thiol-H was modified on the modified electrode interface, the redox peak decreased (curve c) due to the repulsion effect between $[Fe(CN)_6]^{3-/4-}$ and the DNA phosphate backbone with negatively charge. Subsequently, the redox peak further decreased (curve d) after incubating with MCH to block the nonspecific site of the sensing interface. Undoubtedly, the redox peak decreased again after incubating the S triggered by the target (curve e), which was attributed to the fact that more negatively charged phosphate backbones were introduced onto the electrode surface. The Fig. S4B demonstrated impedance curves of the stepwise modification process. Compared with the bare GCE (curve a), the value of electron-transfer resistance (Ret) of depAu/GCE decreased (curve b) due to the excellent conductivity of the AuNPs. However, after negatively charged thiol-H (curve c) and blocking agent MCH (curve d) were sequentially modified onto the electrode, the value of Ret increased continually. Moreover, when the electrode was incubated with S, a decreasing trend of Ret was noticed again (curve e), which was ascribed to the increased steric hindrance from the stack of DNA strands. Moreover, the ECL performance of the proposed biosensor was investigated. The bare GCE (curve S4C) has the same negligible ECL response as the electrode modified by H/depAu/GCE (curve S4D). While the modified electrode was incubated with the S related to the target, a high ECL response could be observed (curve S4E). These results confirmed that the superficial construction of proposed biosensor was successful.

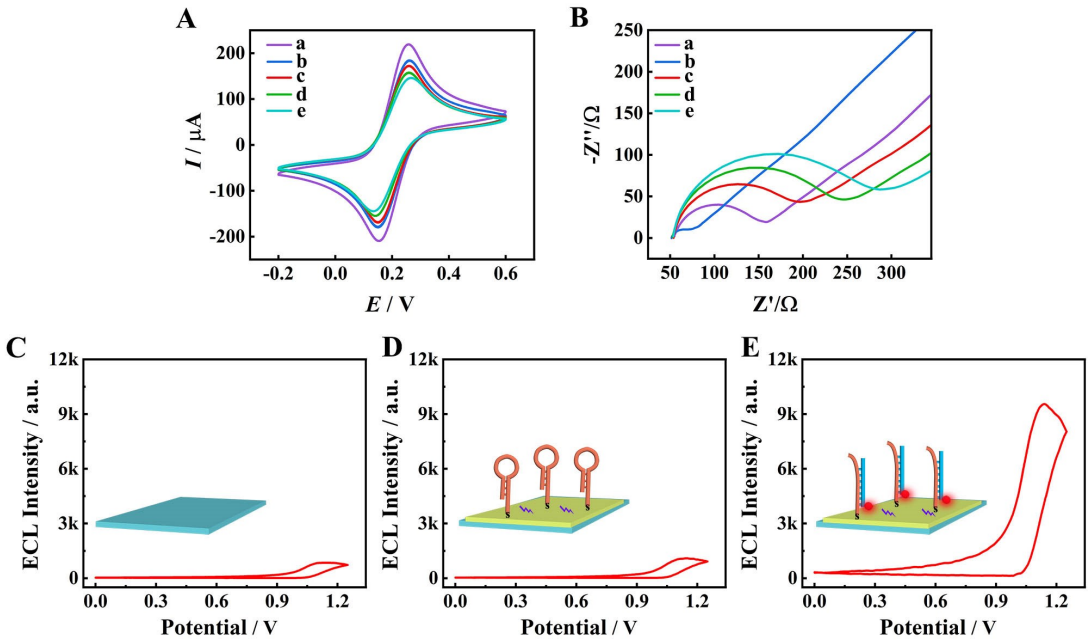

Fig. S4. (A) CV responses and (B) EIS responses of different modified electrodes: (a) bare GCE, (b) depAu/GCE, (c) H/depAu/GCE, (d) MCH/H/depAu/GCE, (e) S/MCH/H3/depAu/GCE. The ECL performance of the biosensor (C) GCE, (D) H/depAu/GCE, (E) S/MCH/H3/depAu/GCE. Detection solution: 2 mL of PBS containing 10 mM Tri-n-propylamine.

The calculation of the density of capture probe on the modified electrode.

the effective electroactive surface area of the modified electrode (depAu/GCE) and the density of capture probe H on the modified electrode were also studied by through cyclic voltammetry (CV) and chronocoulometry (CC). As shown in Fig. S5A, CVs were operated in 5 mM $[Fe(CN)_6]^{3-/4-}$ solution at different potential scan rates (20, 40, 60, 80, 100, 120, 140, 160, 180, 200 and 220 mV/s, respectively). The peak current (I_p) was calculated by the Randles-Sevcik equation.[1,2]

$$I_p = (2.69\times10^5)n^{3/2}AD^{1/2}cv^{1/2} \qquad (1)$$

Then, the linear regression for the peak current (I_p) *versus* the square root of scan

rate ($v^{1/2}$) was presented in Fig. S5B. According to the slope S and the Randles-Sevcik equation，the electroactive area A can be expressed as eqn (2).

$$A = S/(2.69\times10^5)n^{3/2}D^{1/2}c \qquad (2)$$

where n is the number of electrons involved (n=1), D is the diffusion coefficient (6.72×10^{-6} cm^2 s^{-1}, 25 °C), and c is the concentration of ferricyanide (5 mM). Therefore， the electroactive area A of the modified electrode was calculated as 19.2 mm^2.

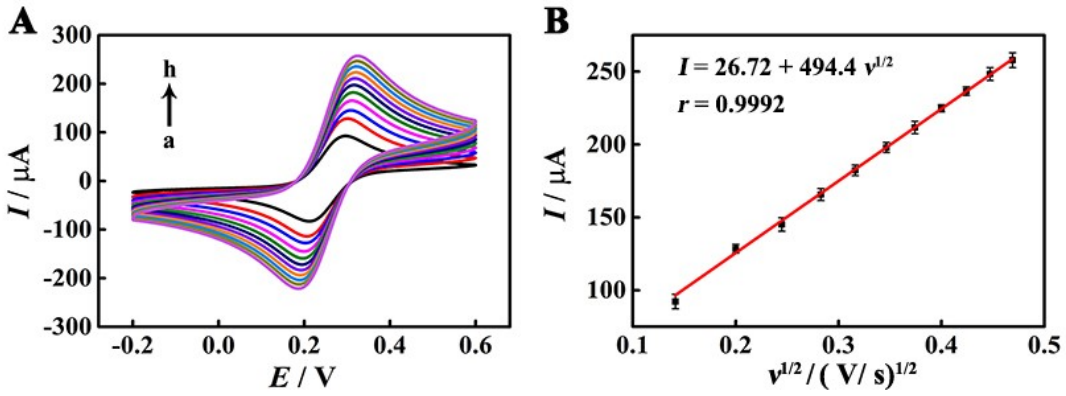

Fig. S5. (A) CVs of depAu/GCE in 5.0 mM $Fe(CN)_6^{3-/4-}$ at different scan rates (a-k: 20, 40, 60, 80, 100, 120, 140, 160, 180, 200 and 220 mV/s); (B) The linear relation of the depAu/GCE with the peak current against the square root of scan rate.

Moreover, the surface coverage of the H on the depAu/GCE can be measured by CC (Fig. S6).[3] The depAu/GCE was first immersed in pure Tris-HCl buffer (10 mM, pH 7.4) to measure the resulting charge flow (curve a). The modified electrode of H/depAu/GCE was then performed in a saturation solution of 50 μM hexaammineruthenium(III) (Ruhex) in Tris-HCl buffer (curve b). Then, the density of H (Γss) could be calculated by using the following eqn (3) and (4).

$$\Gamma_{ss} = (Q_{ss}N_A/nFA)(z/m) \qquad (3)$$

$$Q_{ss} = Q_{total} - Q_{dl} \quad (4)$$

where N_A is Avogadro's number, n is the number of electrons per molecule for reduction, A is the effective surface area of working electrode, z is the charge of the redox molecule and m is the number of nucleotides in the DNA. Q_{total} and Q_{dl} are got from the plot of the charge (Q) versus the square root of scan time ($t^{1/2}$). Thus, the density of H on depAu/GCE in this work was 1.81×10^{13} molecules cm^{-2}.

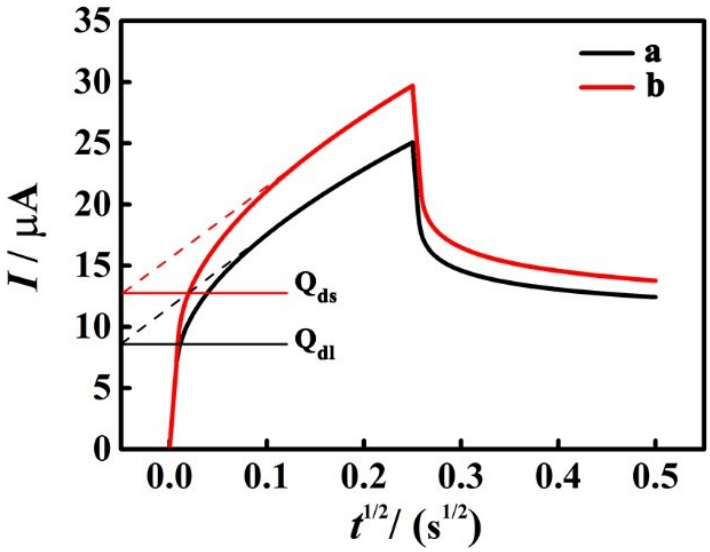

Fig. S6. CC curves of depAu/GCE modified with 3 μM H (a) in Tris-HCl (10 mM, pH 7.4) and (b) in Tris-HCl (10 mM, pH 7.4) including 50 μM RuHex.

Limit of detection calculation for the miRNA biosensing.

According to IUPAC definition, we have calculated the LOD by the following equations, where x_B is the ECL intensity of blank sample and S_B is the standard deviation of blank samples, and IUPAC suggests that $k = 3$ allows a confidence level of 99.86%.[4,5]

$$I_L = x_B + k \times S_B \quad (1)$$

$$I = 1749.29\lg c_{\text{miRNA-21}} + 6078.51 \quad (2)$$

In this paper, specifically, the ECL measurements for blank samples were executed with twenty parallel tests, which exhibited an average ECL intensity of blank sample of 879.62 and a standard deviation (S_B) of blank sample with 305.93. On account of this, the ECL intensity of detection limit (I_L) was estimated to be 1797.42 a.u.. Under the equation of the calibration (2), the estimated detection limit was calculated to be 3.57 aM.

Study on the selectivity of the biosensor for mismatched miRNA-21.

In order to further assess the specificity of our proposed ECL biosensor for target miRNA-21 detection, a series of mismatched sequences of the miRNA-21 including single-base and double-base mismatches were selected as control factors. As depicted in Fig. S7, the relatively low ECL intensity was noticed when the biosensor was incubated with one-mismatched miRNA-21 (10 pM) and double-mismatched miRNA-21 (10 pM). Oppositely, the ECL signal was remarkably increased with the presence of target miRNA-21 (100 fM), even though the concentration of target miRNA-21 was 100 times lower than above mismatched miRNA-21. Besides, the mixed reagents containing 100 fM of target miRNA-21 and mismatched miRNA-21 had been also analyzed with the proposed sensing system, demonstrating an obvious ECL responses as expected. These results furtherly revealed that the proposed ECL assay possessed high specificity for miRNA-21 detection in the presence of these mismatched sequences of the target miRNA-21. The above results furtherly revealed the excellent specificity

of the proposed ECL assay based on the core-brush 3D DNA nanomachine.

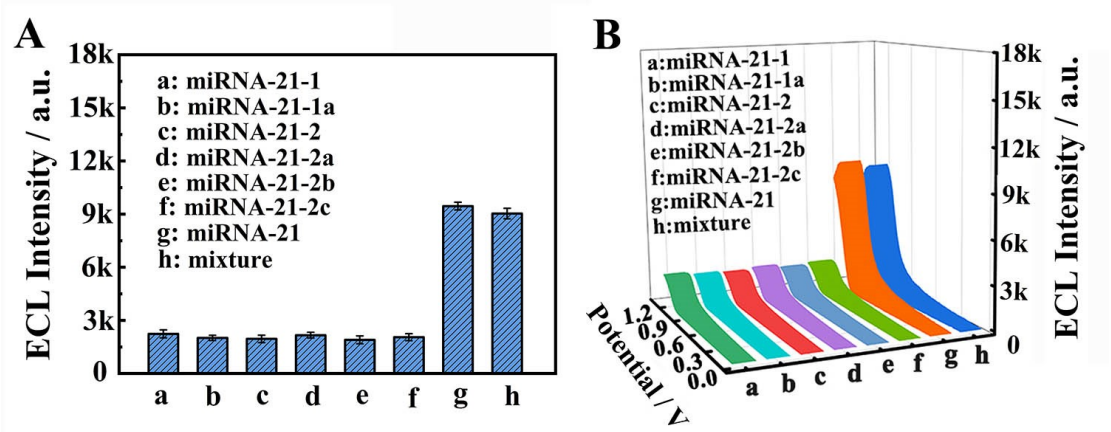

Fig. S7 (A) Specificity and (B) corresponding ECL responses of the proposed strategy for miRNA-21 detection. (a) miRNA-21-1 (10 pM), (b) miRNA-21-1a (10 pM), (c) miRNA-21-2 (10 pM), (d) miRNA-21-2a (10 pM), (e) miRNA-21-2b (10 pM), (f) miRNA-21-2c (10 pM), (g) miRNA-21 (100 fM), (h) mixture.

Table S2. Mismatched sequences of the target miRNA-21.

Names	Sequences (5'-3')
miRNA-21-1	UAG CUU AUC AGA CUG AUG UUU A
miRNA-21-1a	UAG CUU AUG AGA CUG AUG UUG A
miRNA-21-2	UAG CUU AUC AGA CUG GCG UUG A
miRNA-21-2a	UAG CGG AUC AGA CUG AUG UUG A
miRNA-21-2b	UAG CUU AUC AGA CGG AUG AUG A
miRNA-21-2c	UAG CUU UUC AGU CUG AUG UUG A

Stability and reproducibility of the biosensor.

Stability and reproducibility are the significant parameters to evaluate a biosensor. In this study, the ECL emission of the proposed biosensor under continuous potential scanning for 10 cycles was recorded to investigate its stability. As showed in Fig. S8A,

the ECL signal revealed little fluctuation with the relative standard deviation (RDS) of 0.78%, which illustrated nice stability of the proposed biosensor. To apply the core-brush 3D DNA nanomachine to sensing system for a real biomarker detection, a reasonable reproducibility is necessary. As demonstrated in Fig. S8B, the reproducibility of the proposed biosensor was studied by the determination of five different sensing electrodes modified under the same condition, and a relative standard deviation (RSD) of 2.9% was obtained. Furthermore, a batch of electrodes incubated with same miRNA-21 (100 fM) were detected after 7 days, and the RSD was 3.2%. The desirable results indicated that the sensing strategy for biomarker detection exhibited an acceptable reproducibility.

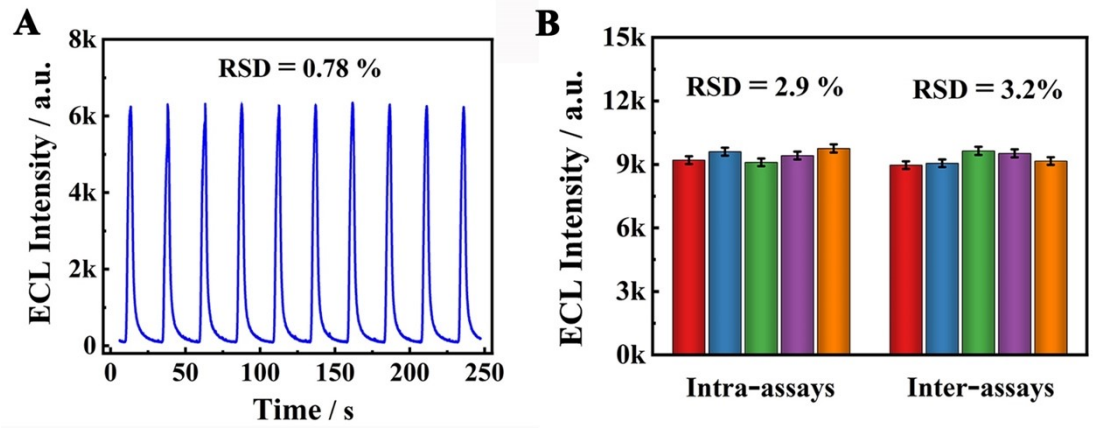

Fig. S8. (A) The stability of the ECL biosensor incubated with 3 μM of capture probe under successive cyclic potential. (B) The reproducibility of the proposed biosensor.

Cellular uptake investigation with inhibitors

To evaluate the uptake mechanism of the core-brush 3D DNA nanomachine, the MCF-7 cells were pretreated with colchicine (inhibitor of macropinocytosis, 5 μg mL^{-1}) and chlorpromazine (inhibitor of clathrin-mediated endocytosis, 5 μg mL^{-1}) for 30

min in a cell culture incubator, respectively. Then, these cells were washed three times with PBS, followed by incubation with the proposed for 4 h at 37 °C. Subsequently, the MCF-7 cells were washed three times with PBS and stained with Hoechst 33342 for 12 min to observe the fluorescence intensity via TIRF microscopy. As depicted in Fig. S9, the cellular uptakes of the core-brush 3D DNA nanomachine in chlorpromazine and colchicine treated MCF-7 cells were approximately decreased to 51% and 46%, respectively, revealing that the core-brush 3D DNA nanomachine entered cells was mainly dependent on clathrin-mediated endocytosis and macro-pinocytosis pathways.

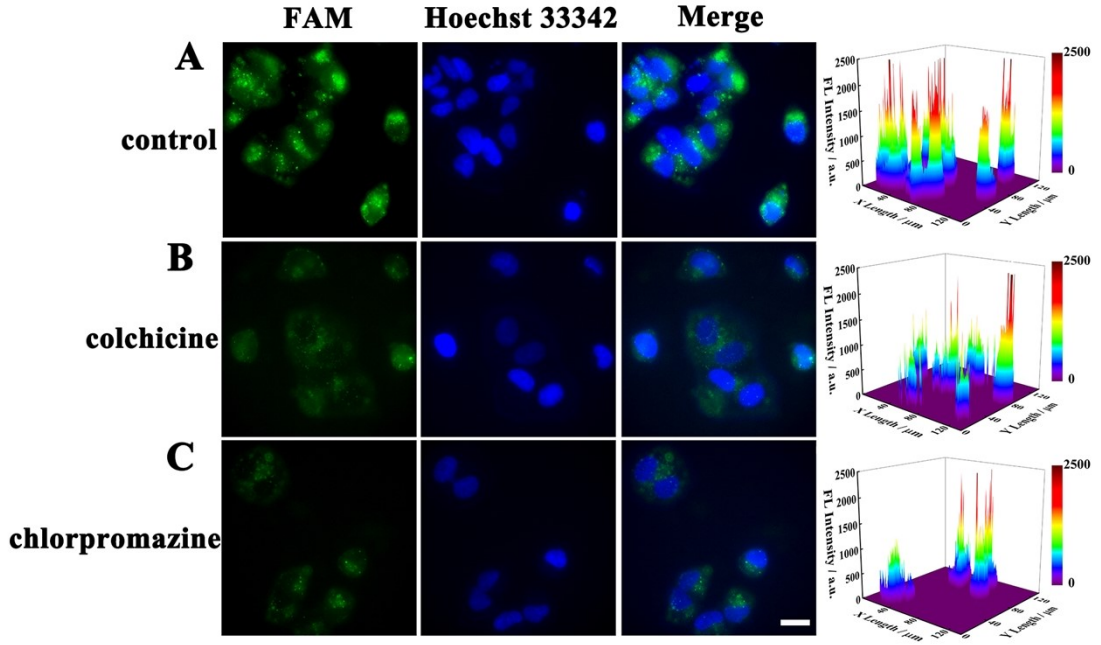

Fig. S9 The TIRF images and the corresponding fluorescence intensities of MCF-7 cells incubated with the core-brush 3D DNA nanomachine. (A) MCF-7 without any treatment was regarded as control. MCF-7 cells were cultured with inhibitors (B) colchicine and (C) chlorpromazine on the cellular uptake of the core-brush 3D DNA nanomachine, respectively. The length of the scale bar is 20 μm.

Cell Viability Assay

MTT assay was performed to evaluate the cytotoxicity of the core-brush 3D DNA nanomachine. Firstly, HeLa cells were cultured in 96-well plates at a density of 1×10^5 cells/well and cultured at 37 °C for 24 h in a humid atmosphere with 5% CO_2. After removed the medium and washed MCF-7 cells twice with PBS, series concentrations of core-brush 3D DNA nanomachine were incubated with HeLa cells for 24 h. The cells were then washed twice with PBS, mixed with 20 μL MTT solution (5 mg/mL) and cultured for 4 h at 37 °C. After removing the remained MTT solution, 150 μL DMSO was added to each well dissolve the formazan crystal precipitates, and the 96-well plate was vibrated slightly for 15 min. The absorbance of each well at 490 nm wavelength was measured via Multiskan Spectrum microplate reader. In addition, MCF-7 cells were also treated with 15mM Mn^{2+} and cultured for different time periods. Then, MTT assay was performed according to above procedure to test the cell viability. As shown in Fig. S10A, negligible cytotoxicity was observed for MCF-7 cells that were treated with core-brush 3D DNA nanomachine at the concentration ranging from 0 to 60 nM, proving the favorable biocompatibility of our nanomachine in biological applications. Furthermore, the indicated concentration of Mn^{2+} didn't influence the viability of MCF-7 cells during the test periods (Fig. S10B). The above results show that our strategy could achieve the intracellular imaging of biomarker.

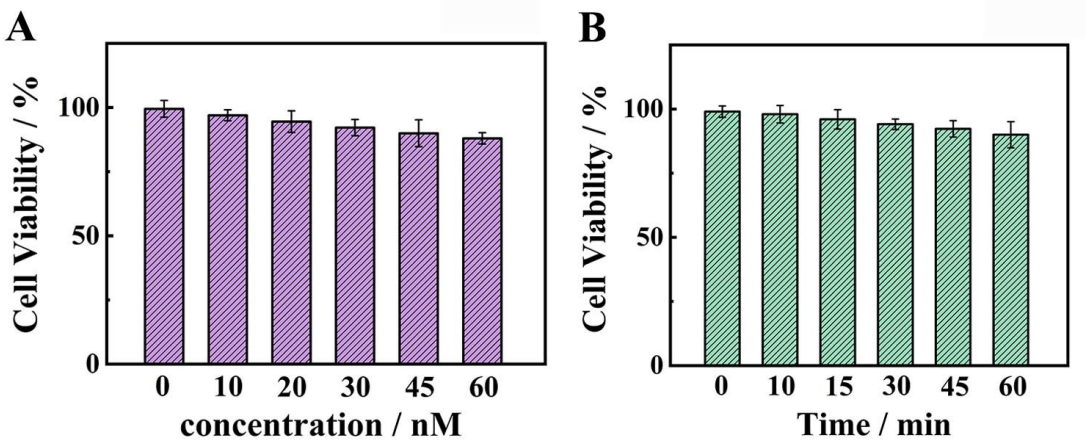

Fig. S10 MTT assays of MCF-7 cells. (A) Cytotoxicity of the core-brush 3D DNA nanomachine with different concentrations. (B) Cell viability of MCF-7 cells incubated with 15mM Mn^{2+} for different time. The error bars indicate means ± S.D. (n=3).

The specific imaging of miRNA-21 in living cells

The specific imaging of miRNA in living cells is of great significance for disease diagnosis and therapeutic effects. Thus, in order to explore the ability of the proposed core-brush 3D DNA nanomachine to specifically distinguish miRNA-21 in living cells, miRNA-21 mimic and miRNA-21 inhibitor were incubated with MCF-7 cells separately to regulate the intracellular miRNA 21 expression. Compared with the fluorescence imaging signal from untreated MCF-7 cells (Fig. S11B), the miRNA-21 mimic treated MCF-7 cells shown obviously enhanced fluorescence (Fig. S11A), while fluorescence intensity was barely observed from the miRNA-21 inhibitor treated MCF-7 cells owing to the decrease of intracellular miRNA-21 expression (Fig. S11C), demonstrating the specific discrimination and quantitative response of the core-brush 3D DNA nanomachine to intracellular miRNA-21. These results suggested that our nanomachine indeed offered reliable toolbox for diagnosis.

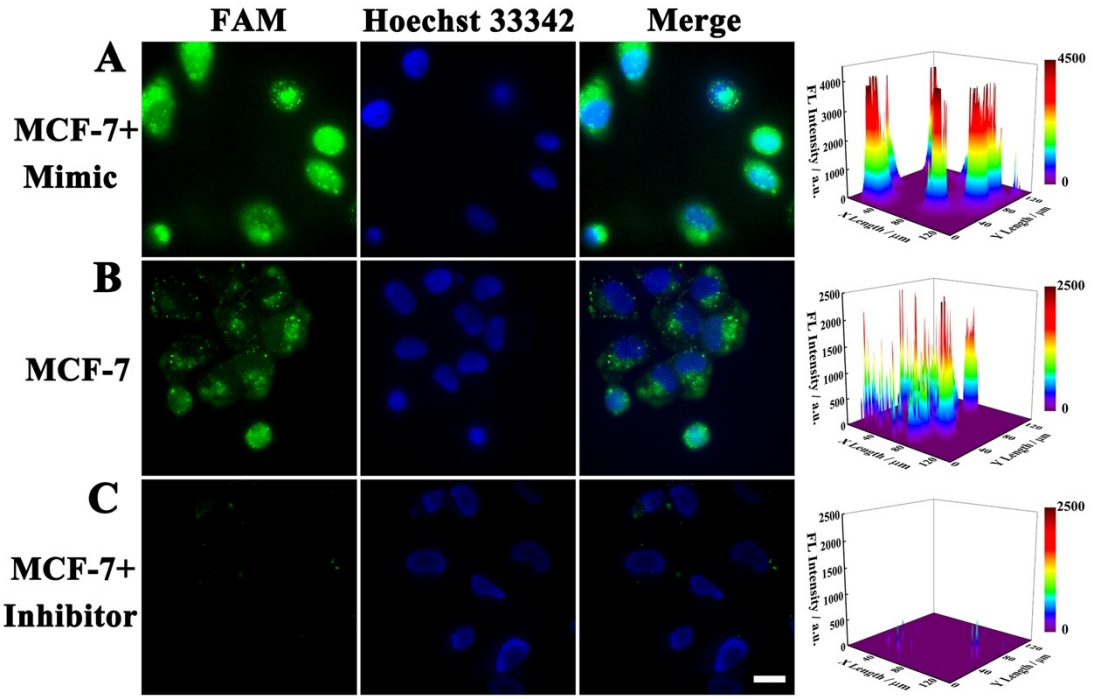

Fig. S11 The TIRF images and the corresponding fluorescence intensities of MCF-7 cells incubated with (A) intact MCF-7 cells, (B) miRNA-21 mimic pretreated MCF-7 cells and (C) miRNA 21 inhibitor pretreated MCF-7 cells, respectively. The length of the scale bar is 20 μm.

Comparison of the biosensor based on the proposed 3D DNA nanomachine with other reported

Table S3. Comparison of the Biosensor Based on the Proposed core-brush structured 3D DNA Nanomachine with Other Reported Works for miRNA Detection.

Detection method	Limit of Detection	Linear range	Ref.
Photoacoustic Imaging	11.69 pM	10 pM-100 nM	6
Electrochemistry	10 pM	0.1 pM-10 nM	7
Fluorescence	22.6 fM	5 fM-10 pM	8
Fluorescence	680 pM	1 nM to 100 nM	9

Electrochemiluminescence	1 fM	1 fM to 100 pM	10
Electrochemiluminescence	6.6 fM	10 fM-0.1 nM	11
Electrochemiluminescence	3.57 aM	10 aM-100 pM	This work

Application of the 3D DNA nanomachine in cell lysates

To evaluate the feasibility of the proposed strategy for miRNA-21 detection in real biological samples, MCF-7 cells and HeLa cells were analyzed for the in *vitro* measurements. As presented in Fig. S12, the ECL intensity gradually increased with the augment of MCF-7 cells concentrations from 10^1 to 10^5. However, the ECL intensity of HeLa cells had low responses and slow growth, which were much lower than those of the MCF-7 cells. The above results confirmed that the miRNA-21 was highly overexpressed in MCF-7 cells and lowly expressed in HeLa cells, which were consistent with previous work.[12-14] Thus, our proposed core-brush 3D DNA nanomachine possessed potential application for distinguishing the different expression levels of miRNAs in the cancer cells.

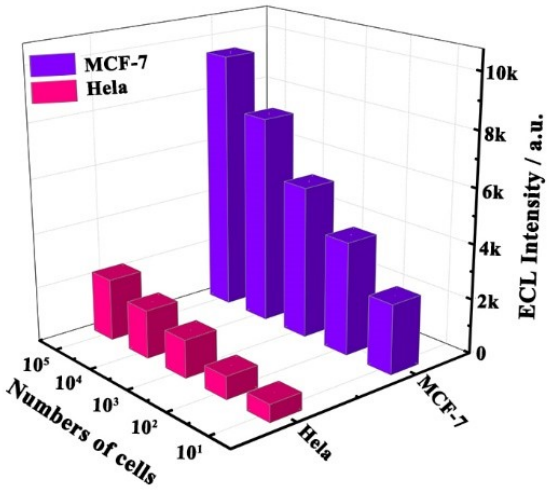

Fig. S12. Practical application of the core-brush structured 3D DNA nanomachine for miRNA-21 detection in diverse cancer-cell lysates.

REFERENCES

1. A. B. Steel, T. M. Herne and M. J. Tarlov, *Anal. Chem.,* 1998, **70,** 4670-4677.
2. J. Shi, J. C. Claussen, E. S. McLamore, A. U. Haque, D. Jaroch, A. R. Diggs, P. Calvo-Marzal, J. L. Rickus and D. M. Porterfield, *Nanotechnol.* 2011, **22,** 355502.
3. J. Zhang, S. Song, L. Wang, D. Pan and C. Fan, *Nat. Protoc.,* 2007, **2,** 2888-2895.
4. W. B. Knighton and E. P. Grimsrud, *Anal. Chem.,* 1983, **55,** 713-718.
5. A. E. Radi, J. L. Sánchez, A. E. Baldrich and C. K. O'Sullivan, *J. Am. Chem. Soc.,* 2006, **128,** 117-124.
6. K. Zhang, X. D. Meng, Z. Yang, Y. Cao, Y. R. Cheng, D. D. Wang, H. T. Lu, Z. J. Shi, H. F. Dong and X. J. Zhang, *Adv. Mater.,* 2019, **31,** 1807888.
7. R. Bruch, J. Baaske, C. Chatelle, M. Meirich, S. Madlener, W. Weber, C. Dincer and G. A. Urban, *Adv. Mater.,* 2019, **31,** 1905311.
8. H. Lee, R. L. Srinivas, A. Gupta and P. S. *Angew. Chem. Int. Ed.,* 2015, **54,** 2477-2481.
9. F. Yang, Y. R. Cheng, Y. Cao, H. F. Dong, H. T. Lu, K. Zhang, X. D. Meng, C. H. Liu and X. J. Zhang, *Chem. Sci.,* 2019, **10,** 1709-1715.

10. T. Zhou, R. Huang, M. Huang, J. Shen, Y. Shan and D. Xing, *Adv. Sci.,* 2020, **7,** 1903661.

11. P. Zhang, J. Jiang, R. Yuan, Y. Zhuo and Y. Q. Chai, *J. Am. Chem. Soc.,* 2018, **140,** 9361-9364.

12. S. Volinia, G. A. Calin, C. G. Liu, S. Ambs, A. Cimmino, F. Petrocca, R. Visone, M. Iorio, C. Roldo, M. Ferracin, R. L. Prueitt, N. Yanaihara, G. Lanza, A. Scarpa, A. Vecchione, M. Negrini, C. C. Harris and C. M. Croce, *Proc. Natl. Acad. Sci. U. S. A.* 2006, **103,** 2257-2261.

13. S. Hu, W. Zhu, L. F. Zhang, M. Pei and M. F. Liu, *Cell Res.,* 2014, **24,** 254-257.

14. Y. Cao, S. Z. Li, C. Chen, D. D. Wang, T. T. Wu, H. F. Dong and Zhang, X. J. *Biomaterials,* 2018, **158,** 23-33.